ISSN(Online): 2320-9801
ISSN (Print): 2320-9798

International Journal of Innovative Research in Computer and Communication Engineering

(An ISO 3297: 2007 Certified Organization)

Website: www.ijircce.com

Vol. 5, Issue 6, June 2017

Robot Manipulator for 3D Surgical Instrument Singulation in Cluttered Environment

Priyanka Pawar, Chetan Neve

M.Tech II year, Dept. of E&TC, Digital System, Govt. Collage of Engineering, Jalgaon, India

ABSTRACT: The aim of seminar is to automate sorting / replenishing items in a hospital using a robot. A unique robotic manipulation system that accurately singulates surgical instruments in a cluttered environment. A novel single view computer vision algorithm identifies the next instrument to grip from a cluttered pile and a compliant electromagnetic gripper picks up the identified instrument. System is validated through extensive experiments. The robot takes user input through serial link about which specific object to be picked up. The source and destination locations are already available in the library of the robot. The robot then autonomously performs the assigned task wherein the robot navigates to the location of the source of the item, identifies the object, picks it up and finally delivers it at the destination location. The navigation is implemented using sensors to find out the distances moved and direction of movement. Object identification has been implemented using image processing techniques. The system also has obstacle avoidance mechanism implemented by use of ultra sonic sensors.

KEYWORDS: unique robotic manipulation system; electromagnetic gripper; ultra sonic sensors; cluttered pile

I. INTRODUCTION

The world needs robots for a number of reasons, including hazardous jobs and automated manufacturing. Robots work without breaks or the need to sleep or eat. Robots also provide a level of precision that is unmatched by the human hand, and one which is repeatable over time frames. An autonomous robot is perform tasks with a high degree of autonomy, which is particularly desirable in fields such as space exploration, household maintenance (such as cleaning), waste water treatment and delivering goods and services. Some modern factory robots are "autonomous" within the strict confines of their direct environment. The factory robot's workplace is challenging and can often contain chaotic, unpredicted variables. The exact orientation and position of the next object of work and (in the more advanced factories) even the type of object and the required task must be determined. This can vary unpredictably (at least from the robot's point of view).

Automatic the preoperative process has the potential to significantly address current safety and efficiency concerns in a hospital. An enabling technology for such is a robotic system that picks and places instruments into bins. Existing approaches to automating the sorting process are expensive and are limited in their capabilities. The state-of- the-art solution, RST's Penelope CS is designed to automate several key functions for the clean side of the sterile supply [9]. A human operator first separates the instruments from a container and places them on a conveyor belt one at a time. Then, a robotic arm fitted with a magnetic gripper picks up a single instrument from the belt. A machine vision system or a barcode scanner is used to identify instruments and sort them into stacks.

It requires additional infrastructure as well as human operation at critical junctures; thus limited in an unstructured. In this report we intend to find a solution for sorting / replenishing items in a store house by automating the system using robots. The issues that need to be catered are as follows:

(a) On receipt of the assigned task, the robot navigates autonomously to the location to pick up the item
(b) Once the robot reaches the item-source location it has to identify the desired item correctly and then pick it up

ISSN(Online): 2320-9801
ISSN (Print): 2320-9798

International Journal of Innovative Research in Computer and Communication Engineering

(An ISO 3297: 2007 Certified Organization)

Website: www.ijircce.com

Vol. 5, Issue 6, June 2017

(c) The robot then navigates to the destination location and drops the item there. obstacles
(d) While navigating the robot should also be able to avoid obstacles contributions include:

- An integrated vision-guided robotic system for simulating surgical instruments from a cluttered environment
- A vision algorithm that identify instruments, estimates 4-DOF poses, and determines the top objects from a pile
- A custom electromagnetic gripper with multi-axis compliance that grips surgical instruments with only a 2D ;location as reference

This paper is an extended version of our previous conference publication [2] through this seminar we intend to build an autonomous robot which navigates through a known given space to locate and detect an object specified by the user and then pick it upt from the particular location and place it at some other desired location. The proposed solution effectively addresses all these challenges and has two key elements: 1) A vision algorithm that robustly identifies the instruments in a clutter, infers the occlusion relationships among the instruments, and provides visual guidance for the robot manipulator. 2) A compliant end-effector design, which can execute precise instrument gripping in a cluttered environment with only a 2D reference point as picking location. This flexibility of the end effectors is important because determining a weak 4-DOF pose (i.e., 2D location, orientation, and scale) in 2D space is more robust and potentially faster than computing an accurate full 6-DOF pose due to the optically challenging nature of the surgical instruments. To our knowledge this is the first instance of an automated sorting solution that is robust to handling a varied instrument suite.

II. RELATED WORK

In recent years, automated tracking of surgical instruments has been gaining popularity (e.g., Key Surgical® KeyDot and Censitrac™). Individual instrument tracking beyond tray level improves infection con- trol and provides a mechanism for root cause analysis. Typically, each surgical instrument is equipped with a small 2D data matrix barcode, which ranges from 1/8 to 1/4 inch in diameter and encodes a unique ID for the tool. We use a commercial barcode reading module to locate and read all visible barcodes from a high-resolution image. We place two barcodes on each side of an instrument, assuming instruments only have two possible stable placements in a pile. For nonflat instrument (e.g., forceps), a cap is used to close the tips, reducing the potential for alternate stable orientations that could limit barcode visibility. On the dirty side, barcode visibility might be affected by biological remains. In such case, the sterile processing nurse will manually remove the instrument from the pile. Fig.2 (a) shows an image of the instruments in a tray and detected barcodes (green boxes).

In a preprocessing step, a library is populated with templates, each of which is an image of an instrument captured with a black background. Each instrument generates two templates in the library one for each side. The templates are indexed using the barcode IDs. Typically, a sterile processing unit has a dirty side and a clean side. On the dirty side, instruments are washed and disinfected manually by a sterile processing nurse. Debris and biological material are re-moved. The job of dirty side robot is to pick up instruments from a pile and sort them into several empty containers based on instrument types (e.g., scissors, tweezers). Then, the nurse brings the containers to a sink, washes the instruments, and brings empty containers back onto the robot's working table for more instruments.

In this research, we use a Baxter Research Robot, whose compliance design allows it to work well with people around. After decontamination, instruments are moved onto the clean side for further processing. The job of the clean side robot is to count the instruments, pick them up, and place them into pre defined locations of a surgical kit. Thus, we use a six-axis Adept® Viper S650 arm, since it is clean room certified and has high accuracy.

ISSN(Online): 2320-9801
ISSN (Print): 2320-9798

International Journal of Innovative Research in Computer and Communication Engineering

(An ISO 3297: 2007 Certified Organization)

Website: www.ijircce.com

Vol. 5, Issue 6, June 2017

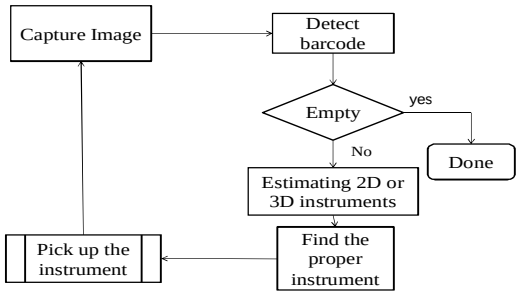

Fig.1 Flowchart of computer vision algorithm for surgical robot

Our vision system is designed for operating on both dirty side and clean side. We use a high resolved region within the robot's work space. Fig.1 shows a flowchart of vision system. The vision algorithm finds one instrument that is a candidate, determines a 2D gripping point, and waits for the robot to pick it up. The process repeats until all instruments are re- moved from the container.

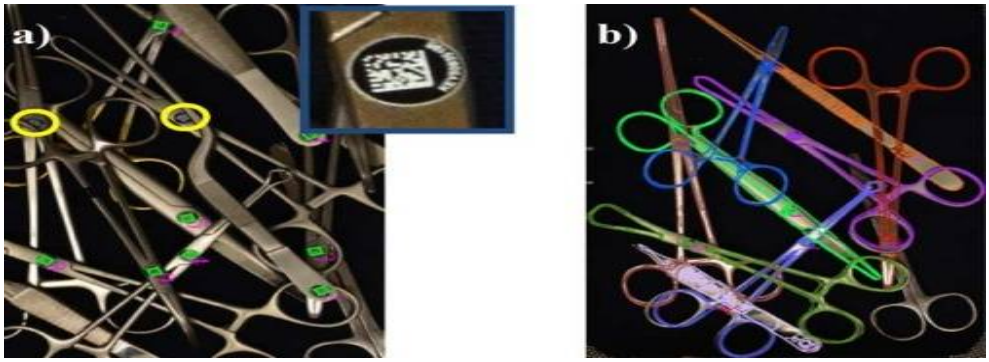

Fig. 2 Transformed template edge maps onto the input image, adopted from [7]

Fig.2 shows a) Decoded barcodes shown in green boxes. There are missed detections due to occlusion (yellow circles). b) Pose estimation using the four corners of the data matrices from both templates and input image. We superimpose transformed template edge maps onto the input image.

III. PROPOSED ALGORITHM

A. *Localization and Post Estimation:*

We estimate a 4-DOF pose for each instrument in an input image. For each detected barcode, we retrieve its counterpart template from the library. The barcode reading module not only reads the ID, but also detects the four corner points of the data matrix. By using the four corners on both the input image and the template, we compute an affine transformation that brings the template into alignment with the instrument in the input image. Fig. 2 (b) shows a visualization of the instrument localization and pose estimation step. We superimpose the randomly colored edges of transformed templates onto the input image to show the effectiveness of alignment.

It is noteworthy that pose estimation can be improved by using either projective transformation or a subsequent nonlinear optimization that minimizes reprojection errors. We simply use affine transform for computational efficiency. As we will discuss later, due to our robust occlusion reasoning algorithm and our compliant end effectors

ISSN(Online): 2320-9801
ISSN (Print): 2320-9798

International Journal of Innovative Research in Computer and Communication Engineering

(An ISO 3297: 2007 Certified Organization)

Website: www.ijircce.com

Vol. 5, Issue 6, June 2017

design, perfect pose estimation is not essential for the success of gripping.

It is noteworthy that pose estimation can be improved by using either projective transformation or a subsequent nonlinear optimization that minimizes reprojection errors. We simply use affine transform for computational efficiency. As we will discuss later, due to our robust occlusion reasoning algorithm and our compliant end effectors design, perfect pose estimation is not essential for the success of gripping.

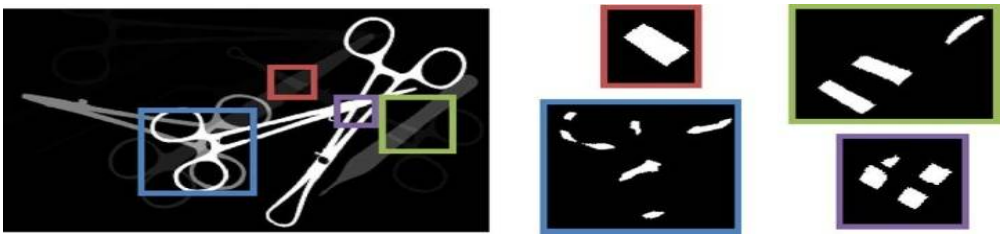

Fig.3 An occupancy map and the intersection region masks between a few pairs of instruments, adopted from [9]

Fig. 3 shows (Left) an occupancy map of the instruments. Instruments that are assigned to a lower bit have lower intensity. (Right) Several binary masks showing pair wise intersection regions between instruments. We first compute a single channel occupancy map. Each bit of the occupancy map is assigned to one instrument. 6

For every pair of intersecting instruments *A* and *B*, there are only two hypothetical occlusion relationships*: A* occludes *B* or *B* occludes *A* (denoted as A > B or B > A) We synthesize two images H_1 and H_2 corresponding to the two hypotheses. This is done by rendering the two templates in different orders. The occlusion relationship can then be inferred by comparing the actual input image against H_1 and H_2. Since H_1 and H_2 only differ at the intersecting regions and are identical, otherwise, we only compare against H_1 and H_2within the intersection region masks. We dilate the masks by a small amount to account for inaccuracy in the estimated poses.

To compare images, we use a descriptor called Edge Orientation Histograms (EOH), which are contrast invariant and only use edges instead of appearance information. To reduce noise and focus on important contour edges, the input images are first blurred with a Gaussian kernel (e.g. 7 X 7). We compute masked EOH (*meoh*) descriptors for image *I*, H_1 and H_2 and then compute Euclidian distances between the histograms. We use 2 X 2 overlapping blocks and 9 bins for each block, resulting in a 36 dimension descriptor. The number of blocks and bins are empirically determined. A thorough study on the parameters can be done in the future to determine the best set of parameters for the descriptor. The hypothesis with smaller histogram distance to the input image *I* is selected:

$$\hat{H} = argmin\ meoh(I) - meoh(H_i)_2 \ \ldots\ldots\ldots\ where\ i = 1,2 \qquad (1)$$

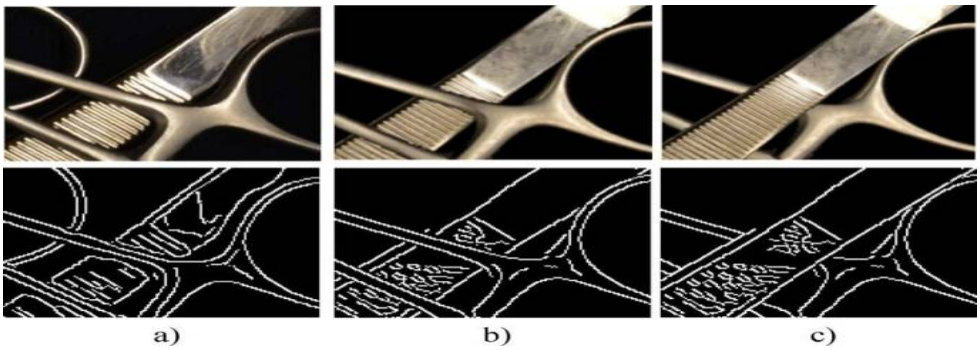

Fig.4 An actual input image and two hypotheses and their edge maps, adopted from [9]

ISSN(Online): 2320-9801
ISSN (Print): 2320-9798

International Journal of Innovative Research in Computer and Communication Engineering

(An ISO 3297: 2007 Certified Organization)

Website: www.ijircce.com

Vol. 5, Issue 6, June 2017

Fig.4 shows an actual image and two hypotheses and their edge maps and a) an input image (top) and a query image generated by Canny edge detection (bottom). b) and c) The two synthesized hypotheses. a) Query Image I. b)H_1. c) H_2 . Due to different lighting condition instruments changed a lot between query image and hypothesis im- ages, especially highlyghts and shadows..

B. *Picking an Instrument:*

Once all the occlusion relationships are determined, the algorithm finds the non-occluded instruments, one of which is randomly selected for picking. Occasionally, all instruments are occluded by others due to an occlusion cycle (e.g A > B > C > A) instrument can be determined empirically by a user in the template creation stage. Since the camera's image plane is parallel to the robot's working surface, the picking location in the image space can be easily translated to the robot's coordinate system. Because of the compliant end-effector design, imperfection in this transformation does not affect gripping accuracy much. Alternatively, an optimal picking location can be determined for the target instrument. For every point on the instrument, we compute the area of the target instrument within a bounding box ofthe size of the gripper, denoted as A_t. We also compute the sum of areas of all other in- struments within the bounding box, denoted as A_0.

$$R=\frac{At}{A0} \qquad (2)$$

The point with the largest R is the optimal picking location. In this way, the contact area between the gripper and instrument is maximized; while the chance of other instruments interfering with the gripping is minimized. A_t and A_0 can be efficiently computed by using integral images on the occupancy map.When the robot fails to grip an instrument, the system will attempt to pick the same instrument twice, before moving on to the next candidate instrument

IV. END EFFECTOR DESIGN

With the end effector of designing a electromagnetic gripper for instrument handling a compliant electromagnetic gripper is designed to grip a surgical instrument in a cluttered environment. The given figure gives the 2D references of the image.

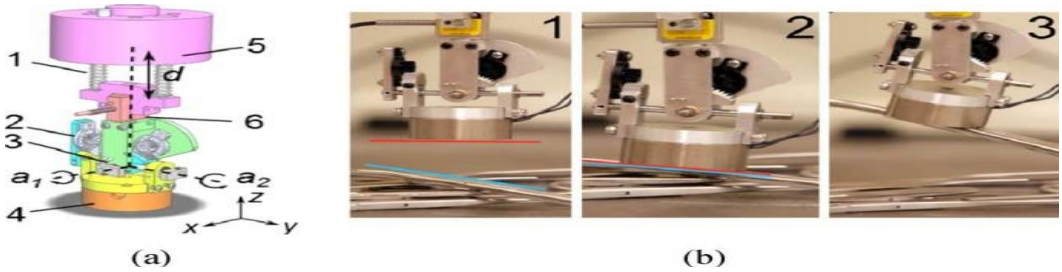

Fig.5 Electromagnetic gripper and workflow of gripping, adopted from [9]

Fig.5 shows (a) Design: 1: Spring for the axis compliance, 2: Rotary damper, 3: Torsion spring, 4: Electromagnet, 5: Adapter, 6: Load cell. (b) Workflow of gripping. The red/blue lines approximate the surface orientation of gripper and instrument before and during contact point as the picking location. As shown in Fig.2.5 (a), the electromagnetic gripper has three passive joints: a prismatic joint along the *z* axis and two revolute joints along the *x* and *y* axes. Each joint has a coil spring attached to the shaft; making these joints compliant. An electromagnet (APW® EM137S) is attached at the bottom of the gripper. To reduce poten- tial adherence between target instrument and adjacent instruments, the current of the electromagnet is modulated by a motor drive to generate a gripping force just enough to pick up the target. For each instrument, the required magnet current is calibrated manually and stored in a lookup table indexed by instrument IDs.

An illustration of instrument pickup work flow is shown in Fig.5 (b). Given a 2D gripping location, a pick-up maneuver is completed with the following three steps:

1) Robot arm moves the gripper to the grip- ping location and at a distance *h* above the instrument. is experimentally determined *h* (e.g., 8 cm) to accommodate various pile height.

ISSN(Online): 2320-9801
ISSN (Print): 2320-9798

International Journal of Innovative Research in Computer and Communication Engineering

(An ISO 3297: 2007 Certified Organization)

Website: www.ijircce.com

Vol. 5, Issue 6, June 2017

2) Robot arm approaches the target along the z axis. When the electromagnet comes in contact with the target, it reorients itself to align with the instrument surface. The robot controller monitors the contact force until F_0 is reached; indicating full contact with the target.
3) The electromagnet is energized to pick up the instrument with a pre-calibrated current. One challenge with electromagnetic gripper is that surgical instruments may be magnetized over time. Residual magnetism not only causes difficulty during surgery, but also leads to drop failure when an instrument adheres to the gripper after the current is set to zero. Our solution is to control the electromagnetic current such that it oscillates and decays over time, i.e.,

$$I = I_0 e^{-t}.\cos \omega t$$

Where I_0 is the electromagnet current for instrument picking. ω is chosen to be 20 for a balanced operation time and π instrument-release success rate. A standard demagnetizer (e.g., Neutrolator®) is also used to demagnetize a tray of instruments after all processing is done. Both Baxter and Viper S650 robots are equipped with our electro-magnetic gripper. For Baxter, an Arduino® Due microcontroller is used as a bridge between the gripper electronics and ROS. For Viper, an Adept® Smartcontroller is used to control the gripper. Communication between the vision system and the robots is via TCP/IP messages.

V. SIMULATION RESULTS

In this section describes the Hough transform for analytic curves of apparatus which should be recognize for the 2D or 3D dimensions of instrument which is in cluttered from . As an example of the parametric version of the transform, we use the ellipse. This example is very important due to the pervasiveness of circles in images, and the fact that a circle becomes an ellipse when rotated about an axis perpendicular to the viewing angle. Despite the importance of ellipses, not much work has used the Hough transform. We consider analytic curves of the form f(x, a) = 0 where x is an image point and a is a parameter vector.

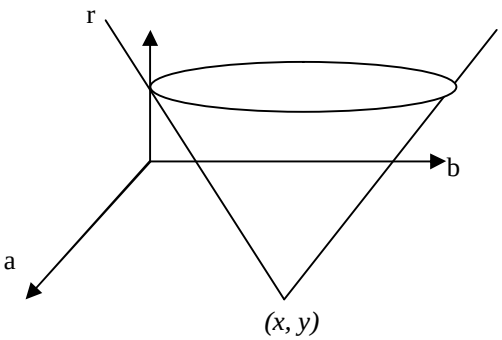

Fig.6 Locus of parameters with no directional information.

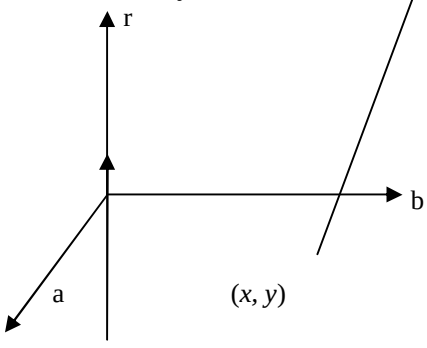

Fig.7 Locus of parameters with directional information

To see how the Hough transform works for such curves, let us suppose we are interested in detecting circular boundaries in an image. In Cartesian co- ordinates, the equation for a circle is given by

$$(x - a)^2 + (y - b)^2 = r^2$$

Suppose also that the image has been transformed into an edge representation so that only the magnitude of local intensity changes is known. This can be seen from equation by treating x and y as fixed and letting, a, b, and r vary. The interesting result about this locus in parameter space is the following. If a set of edge pixels in an image are arranged on a circle with parameters *ao*, *bo*, and *to*, the resultant loci of parameters for each such point will pass through the same point *(ao, bo, to)* in parameter space. Thus many such right circular cones will intersect at a common point.

We see immediately that if we also use the directional information associated with the edge, this reduces the parameter locus to a line, as shown in This is because the centre of the circle for the point *(x, y)* must lie *r* units along

ISSN(Online): 2320-9801
ISSN (Print): 2320-9798

International Journal of Innovative Research in Computer and Communication Engineering

(An ISO 3297: 2007 Certified Organization)

Website: www.ijircce.com

Vol. 5, Issue 6, June 2017

the direction of the gradient. Formally, the circle involves 3 parameters. By using the equation for the circle together with its derivative, the number of free parameters is reduced to one. Formally, what happens is the equation.

$$\frac{df}{dx}(x,a) = 0$$

introduces a term *dy/dx* which is known since

$$\frac{dy}{dx} = \tan\left[\emptyset(x) - \frac{\pi}{2}\right]$$

where, ∅(x) is the gradient direction.

This suggests the following algorithm. Hough algorithm for analytic curves in grey level images. For a specific curve *f(x, a) = O* with parameter vector a, form an array *A(a),* initially set to zero. This array is termed an accumulator array. Then for each edge pixel x, compute all a such that

$$f(x,a) = 0 \ and \ \frac{df}{dx}(x,a) = 0$$

increment the corresponding accumulator array entries:

$$A(a) \coloneqq A(a) + 1$$

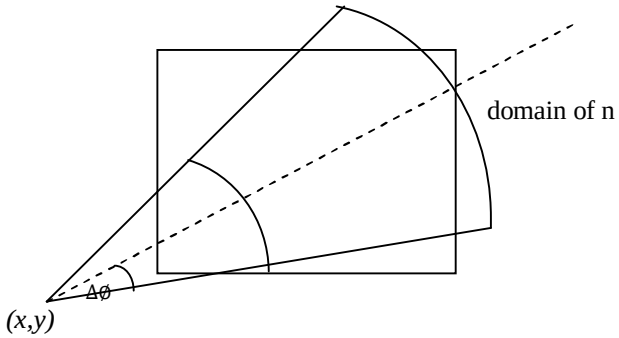

Fig.8 Using convolution templates to compensate for errors.

After each edge pixel *x* has been considered, local maxima in the array *A* correspond to curves off in the image. If only the equation *f(x, a) = 0* is used, the cost of the computation is exponential in the number of parameters minus one, that is, where m parameters each have *M* values, the computation is proportional to M^m- *1*. This is because the equation of the curve can be used to determine the last parameter. The use of gradient directional information saves the cost of another parameter making the total effort proportional to M^m-2, for $m \geq 2$.

A problem arises in detecting maxima in the array A(a). Returning to the initial example of detecting circles, the smoothing of the accumulator array is almost equivalent to the change in the incrementing pro- cedure we would use to allow for uncertainties in the gradient direction ∅ and the radius *r*. If we recognized these uncertainties as,

$$\emptyset(x) \pm \Delta\emptyset$$

$$r \pm \Delta r(r)$$

We would increment all values of a which fall within the shaded band. We let Ar increase with r so that uncertainties are counted on a percentage basis. Suppose we approximate this procedure by incrementing all values of a

ISSN(Online): 2320-9801
ISSN (Print): 2320-9798

International Journal of Innovative Research in Computer and Communication Engineering

(An ISO 3297: 2007 Certified Organization)

Website: www.ijircce.com

Vol. 5, Issue 6, June 2017

which fall inside the square domain centered, according to some point spread function h. After the first contributing pixel which increments center ao has been taken into account, the new accumulator array contents A will be given by

$$A(a) = h(a - a_0)$$

$$where\ a = (a_1\ a_2\ r) \quad a_0 = (a_{10}\ a_{20}\ r_0)$$

If we include all the contributing pixels for that center, denoted by *C*, the accumulator is

$$A(a) = (a_0)h(a - a_0)$$

Finally for all incremented centers, we sum over *ao*:

$$A(a) = \sum_{a_0} c\ (a_0)h(a - a_0)$$

$$\text{but } c(a_0) = A(a_0), \text{so that}$$

$$A(a) = \sum_{a_{11}} A(a_0)h(a - a_0)$$

$$= A^* h = A_s(a)$$

Thus within the approximation of letting the square represent the shaded band shown in Fig.3.3, the smoothing procedure is equivalent to an accommodation for uncertainties in the gradient direction and radius.

In our model, the non-vector space control approach considers the state of the system as a set instead of a vector. A system in the non vector space can be described as

$$\varphi(x(t),\ u(t)) \in \dot{S}(t),$$

where $\dot{S}(t)$, which is different from traditional derivatives with respect to time, is the set of all bounded Lipchitz functions satisfying particular conditions .

$$u(t) = \gamma(S(t))$$

is the feedback mapping from the current feedback set *S(t)*.

Under this general framework, the stabilization problem in the non-vector space can be stated as follows: Given a controlled dynamics system $\varphi(x(t),\ u(t)) \in \dot{S}(t)$, a constant desired set $\hat{S}$, and an initial set S0 in the vicinity of $\hat{S}$, a feedback controller should be designed, $u(t) = \gamma(S(t))$, such that the feedback set S(t) will approach $\hat{S}$ asymptotically. To address this problem, we have devised the following theorem. For the system $f(x)\ u \in \dot{S}(t)$ with $f(x) \in R^{m \times n}$, $x \in R^m$, $u \in R^n$, and $S \subset R^m$, the following controller can locally asymptotically stabilize it at $\hat{S}$:

$$u(t) = \gamma(s) = \left\{ -\alpha \frac{D(s)}{D^T(s)D(S)} \left[\int_s^n d_s^2(x)\, dx + \int_s^n d_s^2(\hat{x})\, d\hat{x} \right] \right\}$$

Where , $d_s^2(x)$ is the projection of a point x to a set *s*.

The detailed form of $D(S) \in Rn$ can be found. The vision-based control problem can be modelled by the system in the above theorem, and the controller can be readily applied. In fact, for serving with greyscale images, each pixel can be represented by a 3D vector

$$x = [x1,x2,x3]^T$$

Where *x1* and *x2* are the pixel indices, and *x3* the pixel intensity.

For a general visual servoing problem, the control input is the camera's spatial velocity. Therefore, the control input, *u(t)*, has three translational components and three rotational components, which can be represented by a vector,

$$u(t) = [vx,vy,vz,\omega x,\omega y,\omega z]^T$$

The system in the theorem is determined by $\varphi(\dot{x})$, which is further determined by the relationship between *u(t)* and *x(t)*.

The perspective-projection-sensing model in computer vision can be used to derive such a relationship. Under constant lighting condition, *x3* will be a constant for each pixel; therefore, $\dot{x}3 = 0$. With a unit camera focal length, a 3D point with coordinates

$$P = [px, py, pz]^T$$

In the camera frame will be projected to the image plane with coordinates $x1 = px/pz$, $x2 = py/pz$. Based on these equations, the relation between *u(t)* and *x(t)* can be obtained as

$$\dot{x}(t) = L(x(t))u(t),$$

where,

ISSN(Online): 2320-9801
ISSN (Print): 2320-9798

International Journal of Innovative Research in Computer and Communication Engineering

(An ISO 3297: 2007 Certified Organization)

Website: www.ijircce.com

Vol. 5, Issue 6, June 2017

$$L = \begin{bmatrix} -1/P_z & 0 & x_1/P_z & x_1x_2 & -(1+x_1^2) & x_2 \\ 0 & -1/P_z & x_2/P_z & (1+x_2^2) & -x_1x_2 & -x_1 \\ 0 & 0 & 0 & 0 & 0 & 0 \end{bmatrix}$$

Note that the first two rows are the same as the interaction matrix in visual servoing. Since $\dot{x}(t) = L(x(t))\, u(t)$ has the same form of the system in the theorem, the controller can be readily applied.

VI. Conclusion and Future Work

We develop a flexible robotic manipulation system that is able to identify and singulate surgical instrument from cluttered tray. The vision algorithm is robust against changing light conditions. The compliant electromagnetic gripper allows us solve for 2D pose instead of more challenging 3D pose. The compliant design of the gripper also makes it possible to recover from certain gripping failures and can be extended to applications involving other mostly planar objects, such as certain industrial parts. In the future, we will first work on error handling. For the scenario a visionbased object verification algorithm can determine whether the topmost object is indeed unoccluded. A verification step using an additional camera can be incorporated to verify if a singulated instrument is indeed the one determined by the vision algorithm. Currently, we require that all the instruments with a pivot be in closed position. In the future, we would like to extend our algorithm to handle opened instruments. This involves identifying the instruments, finding the pivot location, and performing template matching on the two portions separately. In the whole procedure of our seminar work completion we have successfully build android based robot with pick and place robot application.

References

1. A. Pretto, S. Tonello, and E. Menegatti, "Flexible 3D localization of planar objects for industrial bin-picking with monocamera vision system," in Proc. IEEE Int. Conf. Autom. Sci. Eng., 2013, pp. 168–175.
2. C. Choi, Y. Taguchi, O. Tuzel, M.-Y. Liu, and S. Ramalingam, "Voting- based pose estimation for robotic assembly using a 3D sensor," in Proc. IEEE Int. Conf. Robot. Autom., 2012, pp. 1724–1731.
3. C. Papazov, S. Haddadin, S. Parusel, K. Krieger, and D. Burschka, "Rigid 3D geometry matching for grasping of known objects in clut- tered scenes," Int. J. Robot. Res., vol. 31, no. 4, pp. 538–553, Apr. 2012
4. M. Nieuwenhuisen, D. Droeschel, D. Holz, J. Stückler, A. Berner, J. Li, R. Klein, and S. Behnke, "Mobile bin picking with an anthropo- morphic service robot," in Proc. IEEE Int. Conf. Robot. Autom., 2013, pp. 2327–2334.
5. M.-Y. Liu, O. Tuzel, A. Veeraraghavan, Y. Taguchi, T. K. Marks, and R. Chellappa, "Fast object localization and pose estimation in heavy clutter for robotic bin-picking," Int. J. Robot. Res., vol. 31, no. 8, pp. 951–973, Jul. 2012.
6. N. Shroff, Y. Taguchi, O. Tuzel, A. Veeraraghavan, S. Ramalingam, and H. Okuda, "Finding a needle in a specular haystack," in Proc. IEEE Int. Conf. Robot. Autom., 2011, pp. 5963–5970
7. S. Chitta, E. G. Jones, M. Ciocarlie, and K. Hsiao, "Mobile manipu- lation in unstructured environments: Perception, planning, and execu- tion," IEEE Robot. Autom. Mag., vol. 19, no. 2, pp. 58–71, Jun. 2012.
8. X. Wang, T. Han, and S. Yan, "An HOG-LBP human detector with partial occlusion handling," in Proc. IEEE Int. Conf. Comput. Vision, 2009, pp. 32–39.
9. Y. Xu, X. Tong, Y. Mao, W. Griffin, B. Kannan, and L. DeRoose, "A vision guided robot manipulator for surgical instrument singulation in a cluttered environment," in Proc. IEEE Int. Conf. Robot. Autom., 2014, pp. 3517–3523.